European Journal of Chemistry

View Journal Online
View Article Online

Metal(II) triazole complexes: Synthesis, biological evaluation, and analytical characterization using machine learning-based validation

Muhammad Yousaf Arshad [1,2,*], Aqsa Rashid [3], Faisal Mahmood [4], Salaha Saeed [2,5], and Anam Suhail Ahmed [1,6]

[1] *Department of Chemical Engineering, Faculty of Chemical and Petroleum Engineering, University of Engineering and Technology, Lahore, 54000, Pakistan*
[2] *Interloop Limited, Khurrianwala, Faisalabad, 38000, Pakistan*
[3] *Department of Chemistry, Faculty of Applied Sciences, Government College Women University, Faisalabad, 38000, Pakistan*
[4] *Department of Energy Systems Engineering, Faculty of Agricultural Engineering and Technology, University of Agriculture, Faisalabad, 38000, Pakistan*
[5] *Institute of Environmental Engineering and Research, Faculty of Civil Engineering, University of Engineering and Technology, Lahore, 54000, Pakistan*
[6] *Mud-Logging and Well Drilling Department, Halliburton Company, Delaware, 19720, United States of America*

* *Corresponding author at: Department of Chemical Engineering, Faculty of Chemical and Petroleum Engineering, University of Engineering and Technology, Lahore, 54000, Pakistan.*
e-mail: yousaf.arshad96@yahoo.com (M.Y. Arshad).

RESEARCH ARTICLE

10.5155/eurjchem.14.1.155-164.2396

Received: 24 December 2022
Received in revised form: 26 January 2023
Accepted: 06 February 2023
Published online: 31 March 2023
Printed: 31 March 2023

KEYWORDS

Complexes
Fungal strains
Transition metal
Machine learning
K-Nearest neighbors

ABSTRACT

The synthesis of many transition metal complexes containing 3,5-diamino-1,2,4-triazole (Hdatrz) as a ligand with different counter anions Br^-, Cl^-, ClO_4^- and SO_4^{2-} has been studied extensively, but the chemistry of transition metal nitrate and acetate compounds and their reactivity are relatively unexplored. In this research work, two new series of metal(II) complexes (M = Ni, Co, and Zn) {$[Ni_3(Hdatrz)_6(H_2O)_6](NO_3)_6$ (1), $[Co_3(Hdatrz)_6(H_2O)_6](NO_3)_6$ (2), $[Zn_3(Hdatrz)_6(H_2O)_6](NO_3)_6$ (3), $[Ni_3(Hdatrz)_6(H_2O)_6](OAc)_6$ (4), $[Co_3(Hdatrz)_6(H_2O)_6](OAc)_6$ (5) and $[Zn_3(Hdatrz)_6(H_2O)_6](OAc)_6$ (6)} have been synthesized. These synthesized complexes were characterized by various physicochemical techniques such as UV-vis spectroscopy, Fourier transform infrared spectroscopy, and magnetic susceptibility measurements. All six complexes were found to be trinuclear and bridged through the Hdatrz ligand. Spectral data suggested a distorted octahedral environment around the central metal ions in these complexes. It also revealed that the NH and OH groups are involved in hydrogen bonding. These complexes were tested against the fungal strains *Colletotrichum gloeosporioides* and *Aspergillus niger*. These synthesized complexes have not been observed to have antifungal activities. The machine learning K-nearest neighbours evaluates the analytical characteristics and solubility behavior of the metal complexes. Machine learning models provide results with 75% precision.

Cite this: *Eur. J. Chem.* **2023**, *14(1)*, 155-164 **Journal website**: www.eurjchem.com

1. Introduction

Metal-based compounds are essential for the normal functioning of living organisms. Zinc metal plays a role in metabolic pathways in the human body. Its deficiency can cause growth retardation, loss of appetite, and skin changes [1]. Nickel and cobalt are present in edible oils. These metals have antimicrobial and antiviral properties when combined with complex structures such as triazoles [1-3]. Interest in transition metal complexes is increasing as a consequence of the growing demand for new therapeutic drugs from synthetic products [4]. Triazoles are aromatic ligands with three nitrogen atoms, three hydrogen atoms, and two carbon atoms arranged in a ring. These adaptable ligands created substances with explosive, catalytic and magnetic features [5,6]. Figure 1 shows two forms of triazoles [7].

Bidentate and monodentate coordination mechanisms with 1,2,4-triazole have been observed. In monodentate coordination, N_1/N_2 of the triazole ring is linked to the central metal atom. In bidentate coordination, N_1 and N_2 of the triazole ring were attached to the central metal atom [8,9]. Significant hydrogen bonding is facilitated by 1,2,4-triazole, which improves the medicinal qualities of drugs [10]. The derivatives of 1,2,4-triazole have anticancer [11], antimicrobial [12], antidepressant [13] and antioxidant [14] activities. Among medicinal drugs, triazole-based anticancer, antifungal, antiviral, and antibacterial drugs are available on the market [15].

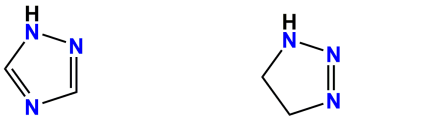

Figure 1. Types of triazoles.

https://dx.doi.org/10.5155/eurjchem.14.1.155-164.2396

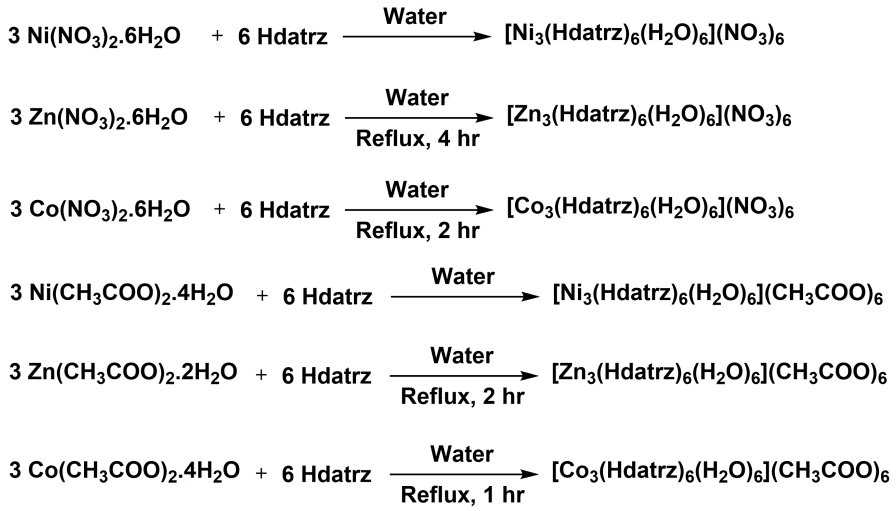

Scheme 1. Synthesis of the complexes.

Coordination complexes formed by the joining of central metal atoms or ion containing empty orbitals with neutral and ionic atoms carrying electron lone pairs (ligand). Metal atoms act as Lewis acid because they are acceptors of the electron pair. Ligands behave as Lewis bases because they are donors of electron pairs. The association of the number of donor atoms with the central atom in a compound is known as the coordination number. Coordination complexes may be neutral, cationic, or anionic. The activity of ligand is usually enhanced by complexation of these metal complexes. The activity of ligand is usually enhanced by complexation and these metal complexes play an important role in modifying the biological properties of compounds [16].

Environmentally friendly nickel, cobalt and zinc nitrate and acetate complexes have been developed with 3,5-diamino-1,2,4-triazole. These transition metal complexes exhibit colors due to *d-d* transitions (at least one electron in the low energy *d* orbital promotes to the high energy *d* orbital [17]. Colored metal complexes, such as copper and nickel complexes, which contain quinolones, are used as an antibacterial agent [18].

Keeping this in mind, in the intended study, divalent transition-metal nitrate and acetate complexes containing 3,5-diamino-1,2,4-triazole were synthesized. We are interested in transition-metal nitrate and acetate complexes with nitrogen donor ligands because they can produce substantial N-H···N hydrogen-bond interactions through strong hydrogen bonding. The synthesized complexes were characterized by magnetic susceptibility measurement, ultraviolet/visible (UV/vis) and infrared spectroscopy. Furthermore, the biological activity of these complexes was analyzed by antifungal tests. The results are validated through the data-driven advance artificial intelligence machine learning (ML) method.

2. Experimental

2.1. Instrumentation

Absorption spectra were recorded on a UV/Vis double beam spectrophotometer, Perkin-Elmer LAMBDA-25 model in the range of 200-1100 nm. FTIR analysis was performed using a FTIR spectrophotometer (Bruker IFS66V/S) to determine the absorption peak within 4000-500 cm^{-1}. The melting points were determined on a digital melting point instrument of the Electro Thermal Model-9200. The magnetic susceptibility was measured with a traditional Gouy balance method, the Sherwood Scientific MK 1 magnetic susceptibility balance.

2.2. Synthesis

2.2.1. Synthesis of $[Ni_3(Hdatrz)_6(H_2O)_6](NO_3)_6$

3,5-Diamino-1,2,4-triazole was purchased from Sigma-Aldrich and used as received. Nickel nitrate hexahydrate (0.290 g, 1 mmol) was added to the aqueous solution of 3,5-diamino-1,2,4-triazole (0.297 g, 3 mmol, Sigma-Aldrich, D26202) with continued stirring. The reaction occurred instantly at room temperature, and the resulting dark blue solution was filtered and allowed to slowly evaporate at room temperature (Scheme 1) [19].

2.2.2. Synthesis of $[Co_3(Hdatrz)_6(H_2O)_6](NO_3)_6$

Cobalt nitrate hexahydrate (0.290 g, 1 mmol) was added to the flat bottom quick-fit flask including 50 mL of an aqueous solution of 3,5-diamino-1,2,4-triazole (0.297 g, 3 mmol) with continued stirring. The color of the solution was red, orange. The reaction mixture was refluxed for 2 h. After 2 hours, a clear dark brown solution was obtained and then evaporated to a third of its original volume on the rotary evaporator. The solution was cooled, filtered, and allowed to stand at room temperature for slow evaporation. After one-month, brown crystals of complex were obtained, which were suitable for single-crystal XRD analysis. Yield: 80%, M.p.: 120 °C (Scheme 1).

2.2.3. Synthesis of $[Zn_3(Hdatrz)_6(H_2O)_6](NO_3)_6$

Zinc nitrate hexahydrate (0.297 g, 1 mmol) was added to the flat bottom quick-fit flask that included 50 mL of an aqueous solution of 3,5-diamino-1,2,4-triazole (0.297 g, 3 mmol) with constant stirring. The reaction mixture was refluxed for 4 hours. After 4 h, precipitation occurred in the reaction mixture. The resulting mixture was cooled, filtered, and precipitates were collected. The color of the precipitates was light brown. Yield: 75%, M.p.: 140 °C, above 250 °C, the synthesized complex was decomposed (Scheme 1).

2.2.4. Synthesis of $[Ni_3(Hdatrz)_6(H_2O)_6](OAc)_6$

Nickel acetate tetrahydrate (0.248 g, 1 mmol) was dissolved in an aqueous solution of 3,5-diamino-1,2,4-triazole (0.297 g, 3 mmol) with continued stirring. The reaction occurred instantly at room temperature, and precipitates occurred in the reaction mixture. The mixture was cooled, filtered and precipitates were collected. The color of the precipitates was dark blue. Yield: 72%, M.p.: 153 °C (Scheme 1).

2.2.5. Synthesis of $[Co_3(Hdatrz)_6(H_2O)_6](OAc)_6$

Cobalt acetate tetrahydrate (0.249 g, 1 mmol) was dissolved in an aqueous solution of 3,5-diamino-1,2,4-triazole (0.297 g, 3 mmol) with continued stirring. Precipitates occurred in the reaction mixture. The mixture was refluxed for 2 h. After 2 hours, a small amount of precipitates remained in the flask. 10 mL of water was added to the flask and the mixture was refluxed for 1 hr. After 1 hour, a clear dark brown solution was obtained. After two days, crystals were obtained. The crystals were dissolved in 10 mL of water and the mixture was refluxed for 1 hr. After 1 h, the mixture was cooled, filtered, and precipitates were collected. The color of the precipitates was dark brown. Yield: 78%, M.p.: 140 °C, however, above 250 °C, the synthesized complex decomposed (Scheme 1).

2.2.6. Synthesis of $[Zn_3(Hdatrz)_6(H_2O)_6](OAc)_6$

Zinc acetate dihydrate (0.219 g, 1 mmol) was dissolved in an aqueous solution of 3,5-diamino-1,2,4-triazole (0.297 g, 3 mmol) with constant stirring. After stirring, bubbling appeared in the flask. 15 mL of water was added to the flask and the mixture was refluxed for 2 h. The mixture was cooled, filtered, and white precipitates of the synthesized complex were collected. Yield: 80%, M.p.: 160 °C (Scheme 1).

2.3. Antifungal activity test

An *in vitro* experiment was carried out to evaluate the antifungal activities of the synthesized complexes to control the growth of *Colletotrichum gloeosporioides* (ATTC 20767) and *Aspergillus niger* (ATTC 10167) fungi using the paper disc diffusion method [20]. For the paper disc diffusion method, 2% potato dextrose agar (PDA) medium was prepared using a standard procedure (200 g potato infusion, 20 g glucose, 20 g agar), autoclaved, and poured into sterile Petri plates. Then 100 µL of *C. gloeosporioides* and *A. niger* spores was evenly spread on the surface of the PDA medium under aseptic conditions. Subsequently, a 6 mm sterile paper disc (Whatman) was loaded with 25 µL of two doses (200 and 300 ppm) of the prepared complexes dissolved in solvents (water and DMSO). The fungicide mancozeb (2 g/L) and sterile distilled water were used as positive and negative controls, respectively. These paper discs loaded with prepared complexes dissolved in solvents (water and DMSO) and control treatments were placed in the center of each Petri plate and were incubated at 26 °C for seven days. A zone of inhibition was recorded 7 days after incubation. The radial diameters of the *C. gloeosporioides* colony and *A. niger* were measured for each treatment petri plate with the help of a ruler (orthogonal measurements) to determine the growth inhibited compared control.

3. Results and discussion

3.1. Electronic absorption spectra of the synthesized complexes

Absorptions at 410, 615 and 950 nm were observed in the electronic absorption spectrum of $[Ni_3(Hdatrz)_6(H_2O)_6](NO_3)_6$. The electronic spectrum showed transitions as follows: ^3A_2g (F) → ^3T_1g (P), ^3A_2g (F) → ^3T_1g (F) and ^3A_2g(F) → ^3T_2g(F), respectively. These absorption values were close to the values recorded for the Ni(II) complex, $[Ni(L)(OAc)]\cdot 3H_2O$, where L stands for the Schiff base ligand containing 1,2,4-triazole. Therefore, these transitions confirmed the distorted octahedral geometry of the Ni(II) complex. The peak at 355 nm was assigned to the ligand to metal charge transfer [21].

The absorption spectrum of $[Co_3(Hdatrz)_6(H_2O)_6](NO_3)_6$ exhibited three absorption peaks at 450, 620 and 980 nm, which were assigned to ^4T_1g (F) → ^4T_1g (P), ^4T_1g (F) → $^4A_2$ g (F) and ^4T_1g (F) → ^4T_2g (F), respectively. These absorption values correspond to the literature values reported for the Co(II) complex, $[Co(L)(OAc)]\cdot 3H_2O$, where L stands for the Schiff base ligand containing 1,2,4-triazole. These transitions are linked to the distorted octahedral geometry of the Co(II) complex. The peak at 336 nm was designated to ligand to metal charge transfer [22]. Absorption at 207 nm was attributed to ligand to metal charge transfer for $[Zn_3(Hdatrz)_6(H_2O)_6](NO_3)_6$. No *d-d* transitions occurred in the visible region. These values were closely related to the values recorded for $[ZnL_2]$ (L: 4-Amino-5-pyridyl)-4*H*-1,2,4-triazole-3-thiol) [7]. The electronic spectrum of $[Ni_3(Hdatrz)_6(H_2O)_6](OAc)_6$ showed three absorption peaks at 420, 625 and 970 nm. These values were assigned to ^3A_2g (F) → ^3T_1g(P), ^3A_2g (F) → ^3T_1g (F) and ^3A_2g(F) → ^3T_2g(F) transitions, respectively. These absorption values were in accordance with the reported Ni(II) complex, $[Ni(L)(OAc)]\cdot 3H_2O$, indicating the distorted octahedral geometry of the Ni (II) complex [21]. The peak at 365 nm was allocated to ligand to metal charge transfer. The absorption peaks at 460, 630 and 930 nm for the complex $[Co_3(Hdatrz)_6(H_2O)_6](OAc)_6$ were assigned to the ^4T_1g (F) → ^4T_1g (P), ^4T_1g (F) → ^4A_2g (F) and ^4T_1g (F) → ^4T_2g (F) transitions, respectively. The distorted octahedral geometry of the Co(II) complex was confirmed by these transitions. These absorption values were comparable to the values recorded for the cobalt complex, $[Co(L)(OAc)]\cdot 3H_2O$. The peak at 346 nm was entitled to ligand to metal charge transfer [22]. The absorbent value at 209 nm for $[Zn_3(Hdatrz)_6(H_2O)_6](OAc)_6$ was appointed as ligand to metal charge transfer. No *d-d* transitions occurred in the visible region. This absorption value was in accordance with the zinc complex, $[ZnL_2]$ (L: 4-Amino-5-pyridyl)-4*H*-1,2,4-triazole-3-thiol) [7].

3.2. Magnetic susceptibility measurements of the synthesized complexes

Magnetic susceptibility measurements of all synthesized complexes are in accordance with the trinuclear nature of these complexes. Magnetic measurements for the $[Ni_3(Hdatrz)_6(H_2O)_6](NO_3)_6$ complex have shown a magnetic moment value (3.6 B.M.) that corresponds to the two unpaired electrons in the *d* orbital in a distorted octahedral structure. It showed the paramagnetic nature of Ni(II) complex. This value is very close to the value recorded for $[Ni_3(pytrz)_8(H_2O)_4](NO_3)_6$, where pytrz stands for 4-(2-pyridyl)-1,2,4-triazole [23].

Magnetic moment measurements for the solid $[Co_3(Hdatrz)_6(H_2O)_6](NO_3)_6$ complex have shown a magnetic moment value of 4.4 B.M. This corresponds to the magnetic moment value of the reported cobalt complex $[Co_2(atrz)_3(mal)_2(H_2O)_2].4H_2O$, where atrz stands for 4-amino-1,2,4-triazole and mal stands for malonic acid [24]. This value is comparable to that of three unpaired electrons suggesting a distorted octahedral geometry around the cobalt(II) complex.

Magnetic susceptibility measurements for the $[Zn_3(Hdatrz)_6(H_2O)_6](NO_3)_6$ complex showed a zero magnetic moment value indicating the diamagnetic behavior of this complex because of d^{10} configuration of Zn(II) metal ion. This value is very similar to the value recorded for the reported zinc complex, $[ZnL_2]$ (L: 4-Amino-5-pyridyl)-4*H*-1,2,4-triazole-3-thiol) [7].

Magnetic measurements for the $[Ni_3(Hdatrz)_6(H_2O)_6](OAc)_6$ complex have shown a magnetic moment value of 3.5 B.M., which is relevant to the value recorded for $[Ni(L)(OAc)]_3\cdot H_2O$, where L stands for Schiff base ligand containing 1,2,4-triazole [22]. This value has suggested the two unpaired electrons in the *d*-orbital and distorted octahedral geometry around the Ni(II) complex.

The magnetic moment value (4.8 B.M.) for $[Co_3(Hdatrz)_6(H_2O)_6](OAc)_6$ complex agrees with three unpaired electrons in the *d* orbital in distorted octahedral structure. Interestingly, this value is not far from the value recorded for $[Co(L)(OAc)]\cdot 3H_2O$ where L stands for the Schiff base ligand containing 1,2,4-triazole [22].

Magnetic susceptibility values of Ni(II) and Co(II) complexes have shown their paramagnetic behavior. The magnetic moment value for the $[Zn_3(Hdatrz)_6(H_2O)_6](OAc)_6$ complex is zero, indicating the diamagnetic behavior of the zinc ion in the +2 oxidation state, which is in accordance with the zinc complex reported, $[ZnL_2]$ (L: 4-Amino-5-pyridyl)-4*H*-1,2,4-triazole-3-thiol) [7].

3.3. Infrared spectroscopy of the synthesized complexes

The infrared spectra of the synthesized complexes demonstrate characteristic bands that are consistent with the functional groups of 3,5-diamino-1,2,4-triazole. The infrared spectrum of the $[Ni_3(Hdatrz)_6(H_2O)_6](NO_3)_6$ complex was analyzed and revealed two broad bands at 3320 and 3450 cm^{-1}, which correspond to OH and NH stretching vibrations, respectively. These peaks serve as evidence for the presence of hydrogen bonding within the complex [25]. The infrared spectra of the ligand exhibit a peak at 1628 cm^{-1}, which may be assigned to the stretching vibrations of C=N. For the complex, this peak has been shifted to 1624 cm^{-1} (sharp peak), which indicates a lowering of the stretching frequency of C=N and the coordination of N_1 and N_2 of the triazole ring with the metal atom [26]. Additionally, the weak band at 564 cm^{-1} indicates stretching vibrations of the metal-nitrogen bond (M-N) [27], while a strong peak at 1338 cm^{-1} indicates stretching vibrations of the nitrate group [28]. The sharp peak at 1034 cm^{-1} is indicative of N-N stretching vibrations [29].

The infrared spectrum of the $[Co_3(Hdatrz)_6(H_2O)_6](NO_3)_6$ complex was analyzed and revealed two weak bands at 3308 and 3450 cm^{-1}, which correspond to stretching vibrations of OH and NH, respectively. These vibrations serve as evidence for the presence of hydrogen bonding within the complex [30]. Additionally, a weak band at 574 cm^{-1} was observed and assigned to symmetric vibrations of the M-N bond [27]. Furthermore, a shift in the band from 1483 cm^{-1} for the ligand to 1470 cm^{-1} (of medium intensity) for the cobalt complex, which was assigned to symmetric stretching vibrations of the nitrate group. This value is notably similar to that recorded for $[Co_3(\mu_2\text{-}Hdatrz)_6(H_2O)_6](NO_3)_8{\cdot}4H_2O$ [31]. Additionally, a medium peak at 940 cm^{-1} was observed, which was indicative of the stretching vibrations of N-N [29].

The band appeared at 3308 and 3460 cm^{-1} for $[Zn_3(Hdatrz)_6(H_2O)_6](NO_3)_6$ indicate O-H and N-H stretching vibrations. These vibrations have confirmed the presence of hydrogen bonds in the zinc complex [31]. The shift in band from 1628 cm^{-1} for the free ligand to 1622 cm^{-1} (sharp band) for the zinc complex, is assigned to stretching vibrations of C=N of the triazole ring, indicating the coordination of N_1 and N_2 of the triazole ring with the metal atom. This coordination of nitrogen atoms of the triazole ring with a metal atom is associated with a lower stretching frequency of C=N [32]. The weak band at 578 cm^{-1} is assigned to the stretching vibrations of the metal-nitrogen bond (M-N) [27]. The strong peak at 1339 cm^{-1} has shown the stretching vibrations of the nitrate group [28]. The peak at 1031 cm^{-1} has indicated the stretching vibrations of N-N [29].

The infrared spectrum of $[Ni_3(Hdatrz)_6(H_2O)_6](OAc)_6$ complex exhibited characteristic bands consistent with the functional groups of 3,5-diamino-1,2,4-triazole, including a broad band at 3307 and 3430 cm^{-1} indicating OH and NH stretching vibrations, respectively. These peaks serve as evidence for the presence of hydrogen bonding within the complex [33]. The strong peak at 1623 cm^{-1} is assigned to the stretching vibrations of C=N, indicating coordination of N_1 and N_2 of the triazole ring with the nickel atom. This shift in frequency is associated with the coordination of the nitrogen atoms of the triazole ring [26]. Furthermore, a weak band at 574 cm^{-1} confirms the stretching vibrations of the metal-nitrogen bond [27]. A strong peak at 1344 cm^{-1} is assigned to the symmetric stretching vibrations of the acetate group [34]. These values are very close to the values recorded for $[Ni(L)(OAc)]{\cdot}3H_2O$, where L represents the Schiff base ligand containing 1,2,4-triazole [22].

The infrared spectrum of $[Co_3(Hdatrz)_6(H_2O)_6](OAc)_6$ shows two broad bands at 3307 and 3500 cm^{-1}, which are assigned to stretching vibrations of O-H and N-H. These vibrations have indicated the presence of hydrogen bonds in the cobalt complex [35]. A strong peak at 1622 cm^{-1} is associated with stretching vibrations of C=N of the triazole ring. This value has confirmed the coordination of the nitrogen atoms of the triazole ring to the metal atom by lowering the stretching frequency of C=N [26]. The weak band at 572 cm^{-1} has confirmed the stretching vibrations of the metal-nitrogen bond [27]. The strong peak at 1339 cm^{-1} has shown the stretching vibrations of the acetate group [34]. These values are very close to the values that are recorded for $[Co(L)(OAc)]{\cdot}3H_2O$, where L stands for the Schiff base ligand containing 1,2,4-triazole [22].

The infrared spectrum of $[Zn_3(Hdatrz)_6(H_2O)_6](OAc)_6$ exposes two broad bands at 3332 and 3490 cm^{-1}, which are indicative of the stretching vibrations of OH and NH. These bands confirm the presence of hydrogen bonds within the zinc complex [36]. The peak at 1574 cm^{-1} has been assigned to the stretching vibrations of C=N, which is indicative of the coordination of N_1 and N_2 of the triazole ring with the metal atom. This coordination is characterized by a lowering of the stretching frequency of C=N [32]. The weak band at 577 cm^{-1} confirms the stretching vibrations of the metal-nitrogen bond [27]. The strong peak at 1339 cm^{-1} is associated with the symmetric stretching vibrations of the carboxylate group of the acetate anion [34]. These values are in close agreement with those recorded for $[Zn(L)(OAc)]{\cdot}3H_2O$ [22].

3.4. Biological activity

The ligand 3,5-diamino-1,2,4-triazole and the synthesized complexes have been tested against fungal strains *C. gloeosporioides* and *A. niger*. These compounds showed zero activity against these fungal species. A similar *in vitro* experiment was carried out with previously reported Ni(II) and Zn(II) complexes to determine their antifungal activities against *A. niger* [37], while Co(II) complex, which contains the triazole Schiff base ligand derived from condensation of 4-amino-5-phenyl-4*H*-1,2,4-triazole-3-thiol with salicylaldehyde, showed effective antifungal activity with a zone of inhibition [38].

3.5. Solubility of synthesized complexes

The solubility of synthesized complexes was determined by dissolving precipitates of these complexes into different solvents. The solubility test values obtained are given in Table 1.

3.6. K-nearest neighbor (K-NN) machine learning validation for the solubility of synthesized complexes

Machine learning (ML) is an advanced statistical tool to analyse complex datasets and deduce optimized decisions [39,40] (Figure 2). ML is divided into three types of mainly (a) supervised ML, (b) non-supervised ML, and (c) reinforcement learning [40]. Supervised ML is easy to implement and is compared to other types of ML. It fits data as per algorithm predefined function *i.e.*, backward substitution and Gaussian regressions [41,42]. Unsupervised ML is deduction of error and decision without particular feedback recognized, while re-enforcement learning is a reward-based agent to data-set optimization [42].

Table 1. Solubility of synthesized complexes in different solvents *.

Complex	Solvents						
	Water	Ethanol	Methanol	Acetone	DCM	DMF	DMSO
$[Ni_3(Hdatrz)_6(H_2O)_6](NO_3)_6$	S	SS	S	IS	-	S	-
$[Co_3(Hdatrz)_6(H_2O)_6](NO_3)_6$	IS	IS	IS	IS	IS	IS	IS
$[Zn_3(Hdatrz)_6(H_2O)_6](NO_3)_6$	S	SS	SS	SS	S	S	-
$[Ni_3(Hdatrz)_6(H_2O)_6](OAc)_6$	SS	IS	IS	IS	IS	IS	SS
$[Co_3(Hdatrz)_6(H_2O)_6](OAc)_6$	IS	IS	IS	IS	IS	IS	IS
$[Zn_3(Hdatrz)_6(H_2O)_6](OAc)_6$	IS	SS	SS	SS	IS	S	SS

* S: Soluble, IS: Insoluble, SS: Sparingly soluble.

Table 2. Data processing and selecting of solubility of synthesized complexes in solvents (1: Soluble (S), 0: Insoluble (IS)).

KNN data set				
No	Complex	Absorption band (nm)	Magnetic moment (B.M.)	Experimental results of solubility
1	$[Zn_3(Hdatrz)_6(H_2O)_6](NO_3)_6$	207	0.0	1
2	$[Ni_3(Hdatrz)_6(H_2O)_6](NO_3)_6$	410	3.6	1
3	$[Co_3(Hdatrz)_6(H_2O)_6](NO_3)_6$	450	4.4	0
4	$[Co_3(Hdatrz)_6(H_2O)_6](OAc)_6$	460	4.8	0
5	$[Ni_3(Hdatrz)_6(H_2O)_6](NO_3)_6$	615	3.6	1
6	$[Co_3(Hdatrz)_6(H_2O)_6](NO_3)_6$	620	4.4	0
7	$[Co_3(Hdatrz)_6(H_2O)_6](OAc)_6$	680	4.8	0
8	$[Co_3(Hdatrz)_6(H_2O)_6](OAc)_6$	930	4.8	0
9	$[Ni_3(Hdatrz)_6(H_2O)_6](NO_3)_6$	950	3.6	1
10	$[Co_3(Hdatrz)_6(H_2O)_6](NO_3)_6$	980	4.4	0

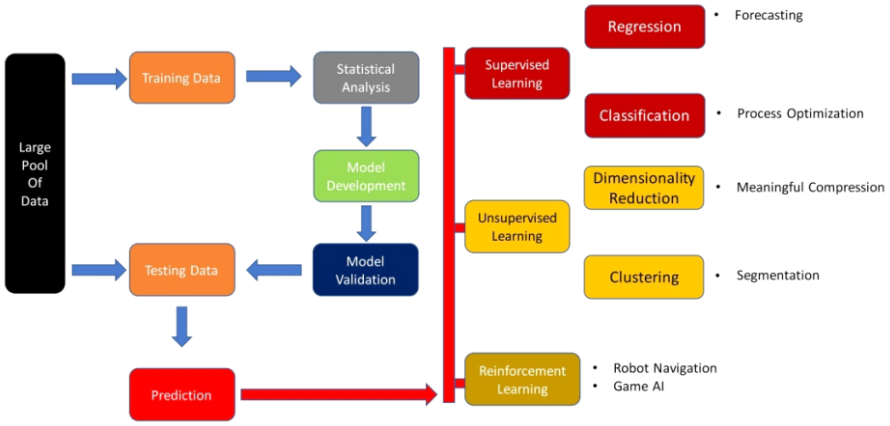

Figure 2. Machine learning flow chart.

In our current research, a variety of datasets are involved, mainly comprised of absorption bands, magnetic moments, and biofouling as per UV and IR spectroscopic analytical techniques. These datasets are noisy and have a peculiar nature, because of the dependence of interlinked molecular components. The solubility of complexes is characterized as soluble, sparingly soluble, and insoluble nature of complexes in organic and inorganic solvents, commonly referred to as instance-based supervised data sets. The solubility experimentation data set has the ability to channelize the solubility characteristic according to the distance between soluble data sets points and insoluble data points of different complexes in multiple solvents.

The KNN algorithm [43,44] is a class of supervised ML and solves regression and classification problems simultaneously. In classification ML, discrete outputs are available in 1 or 0 numbers, usually terms such as class segmentations, yet distinct. KNN designates the neighboring proximity of similar classes in a close vicinity. It creates an assumption based on the true and false events of the problem dataset [44]. True events incur as a useful outcome and supports similarity, proximity in distance, and closeness with neighbouring data points. The distance measure between close points is referred to as the Euclidian support distance. The flow chart of the KNN algorithms for the problem of solubility data and the analysis of the decision tree is shown in Figure 3.

Table 2 highlights the categorical classification of experimental data sets in organic and inorganic solvents, mainly water, ethanol, and DMF. To enhance the computation time, sparingly soluble complexes are referred to as soluble and denoted by 1's. Python Anaconda version 3.7 is used as an interpreter [45,46]. Seaborne, Pandas, Scikit, and Matplotlib libraries of Python are used extensively in ML algorithm implementation [46].

Data pre-processing is the foremost step in the kNN algorithm. It includes the detection of outliers, noisy data hotspots, increasing data quality, and derive useful information from datasets. The accuracy and efficiency of the ML model depends on the accurate data pre-processing. In solubility studies, Figure 4a shows the pair plot for the dependency of the data, and Figure 4a depicts absolute hue graph plots indicates that the magnetic moment data points are highly aligned with absorption band of complexes up to significant scale. Both parametric constraints show nonlinear behavior against the solubility data sets of complexes. It indicates that a simple and multiple linear regression is not of appropriate implication in our problem. The KNN algorithm has a hybrid regime to support the regression and classification problem datasets, as indicated in Figure 5.

Figure 5 highlights the magnetic moments and absorption band dependence on the solubility data points either linearly or non-linearly. K is randomly chosen as 0 and increases as the algorithm proceeds. K indicates the neighboring data points for the calculation of the Euclidean distance. The K values increase the proximity. Feature classifiers induce the Minkowski metric [47,48] to fit training and testing points in the *x* and *y* data sets.

Table 3. Training and testing data to predict the *y*-values of the solubility of synthesized complexes in solvents where 1: Soluble (S), 0: Insoluble (IS).

X-data Set input 1	X-data Set input 2	X-Train 1	X-Train 2	X-Set 1	X-Set 2	X-test 1	X-test 2	Y-Value	Y-Predicted	Y-test 1	Y-test 2	Y-Training
207	0	-	-	-0.6274	0.35444	-0.6274	0.35444	1	-	-	-	0
410	3.6	-	-	1.30392	-0.1418	1.30392	-0.1418	1	-	-	-	1
450	4.4	-	-	0.00993	-0.1418	0.00993	-0.1418	0	-	-	-	0
460	4.8	1.4198	0.35444	-	-	-	-	0	-	-	-	0
615	3.6	-0.7819	-0.1418	-	-	-	-	1	-	-	-	0
620	4.4	0.26101	0.60255	-	-	-	-	0	-	-	-	1
680	4.8	1.22667	0.60255	-	-	-	-	0	-	-	-	0
930	4.8	-0.5888	0.60255	-	-	-	-	0	0	0	0	-
950	3.6	-1.566	-2.3748	-	-	-	-	1	0	1	1	-
980	4.4	0.02925	0.35444	-	-	-	-	0	0	1	1	-

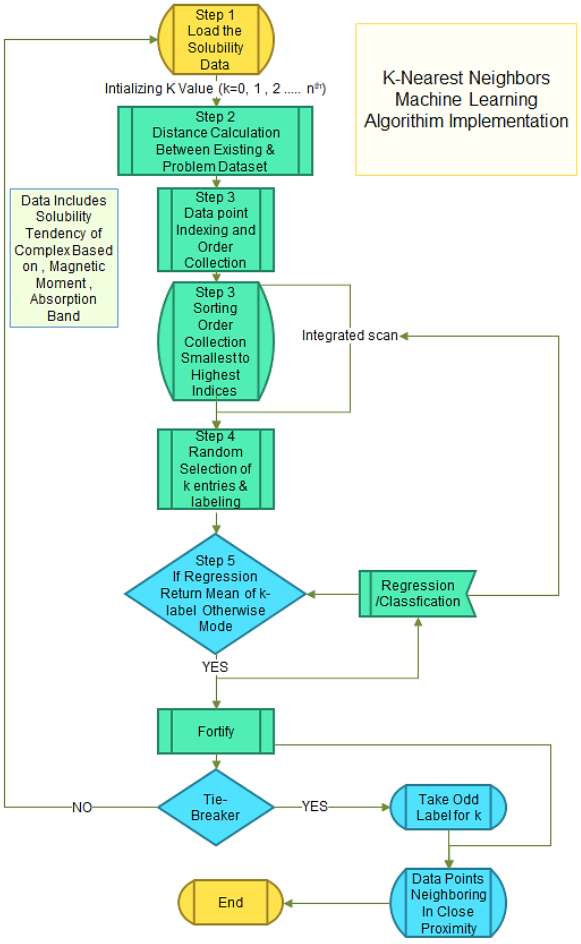

Figure 3. KNN implementation algorithm flow chart for the prediction of the solubility of metal complexes.

Data sets are divided into 70% training data points and 30% testing data points. It indicates the best metric results for p = 8 for the significant neighboring of proximate data points. The y prediction stores the classifier results of the x-testing data points shown in Table 3. A confusion matrix points to the three classical points indicating the exactness in comparison of the experimental results. The Sklearn metric [49] highlights the accuracy of the model at 75%, with three values lying in major true events, as shown in Table 4. To increase the robustness of the model, the data points are randomly divided into set 1 and set 2. It corresponds to the predicted outcomes of y for the given y-test points. It continues to increase at a step rate of 0.01 until the regression error is minimized. For a tie-breaker, an odd data point is taken into consideration. For a normal step size calculation, the mode is highlighted in the proximity of the red and green regions.

The metrics indicate a precision of 0.75 for a recall of the solubility in the organic solvent and 0 for the inorganic solvent and satisfy the experimental data points. The F1 score supports the 3 points for a total of 4 points at a score of 0.86. The true prediction is 33.3% fully confident true event and 66.3% partially true events for the y-set. The KNN algorithm strengthens the data-driven process decision-making to analyse the difference between the variable properties of different complexes in multiple solvents. The generalized datasets provide an in-depth understanding for analytical and expensive procedure conditions validation using advance statistical support.

$[Zn_3(Hdatrz)_6(H_2O)_6](NO_3)_6$ having a band gap of 207 nm with a magnetic moment of 0 is the most confident outcome of the KNN algorithm. $[Co_3(Hdatrz)_6(H_2O)_6](NO_3)_6$ and $[Ni_3(Hdatrz)_6(H_2O)_6](NO_3)_6$ have a greater band number and magnetic moment than $[Zn_3(Hdatrz)_6(H_2O)_6](OAc)_6$ and show a considerable magnetic moment. However, the KNN model predicts the

Table 4. Metrics of solubility of synthesized complexes in solvents for weighted modes, where 1: Soluble (S), 0: Insoluble (IS).

Weighted mode (0,1)	Precision	Recall	F1-score	Support	Confusion matrix	
					True prediction	False prediction
0	0.75	1	0.86	3	1	0
1	0	0	0	1	2	0
Total	0.75	-	0.86	4	-	-
Accuracy	0.75	0.75	0.75	0.75	-	-
Macro average	0.38	0.50	0.43	4	-	-
Weighted average	0.56	0.75	0.64	4	-	-

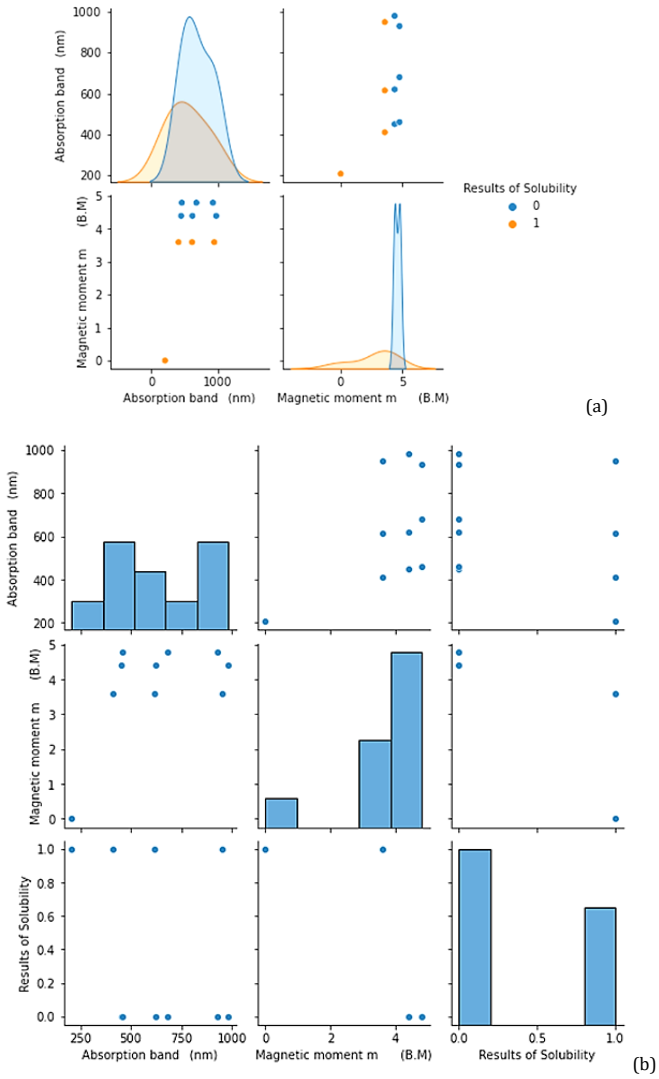

Figure 4. Data analysis and pre-processing of solubility dataset for absorption band, magnetic moment, and results of solubility.

results accurately with a partially true event since the $[Co_3(Hdatrz)_6(H_2O)_6](OAc)_6$ complex is insoluble in organic solvent and the $[Ni_3(Hdatrz)_6(H_2O)_6](OAc)_6$ complex is readily soluble. It signifies that the implemented model shows less variation with increasing magnetic moment and band number. It also shows that the model is equally applicable for solvents both organic and inorganic in nature.

4. Conclusion

The synthesized complexes were characterized by electronic absorption spectroscopy, FTIR spectroscopy, and magnetic susceptibility measurements. FTIR was done to identify peaks of functional groups in the synthesized complexes. The infrared spectra of the complexes predicted the coordination mode of the ligand and the structure of related complexes. Broad peaks appeared in the region of 3000-3500 cm^{-1}, suggesting a hydrogen bond in the molecular structure. Magnetic susceptibility measurements confirmed the number of unpaired electrons and the octahedral geometry of the synthesized complexes. Electronic absorption data of nitrate and acetate bridged Ni(II) complex have three absorptions (410, 615 and 950 nm) that are assigned to the ^3A_2g (F) → ^3T_1g (P), ^3A_2g (F) → ^3T_1g (F) and ^3A_2g → ^3T_2g transitions, respectively. Electronic absorption data of nitrate and acetate bridged Co(II) complex have three absorptions (450, 620 and 980 nm) that are assigned to the ^4T_1g (F) → ^4T_1g (P), ^4T_1g (F) → ^4A_2g (F) and ^4T_1g (F) → ^4T_2g (F) transitions, respectively. These transitions for solid Ni(II) and Co(II) complexes confirmed their octahedral geometry. In light of the physicochemical techniques mentioned above, the structures of the complexes are found to be $[Ni_3(Hdatrz)_6(H_2O)_6](NO_3)_6$, $[Co_3(Hdatrz)_6(H_2O)_6](NO_3)_6$, $[Zn_3(Hdatrz)_6(H_2O)_6](NO_3)_6$, $[Ni_3(Hdatrz)_6(H_2O)_6](OAc)_6$, $[Co_3(Hdatrz)_6(H_2O)_6](OAc)_6]$ and $[Zn_3(Hdatrz)_6(H_2O)_6](OAc)_6$.

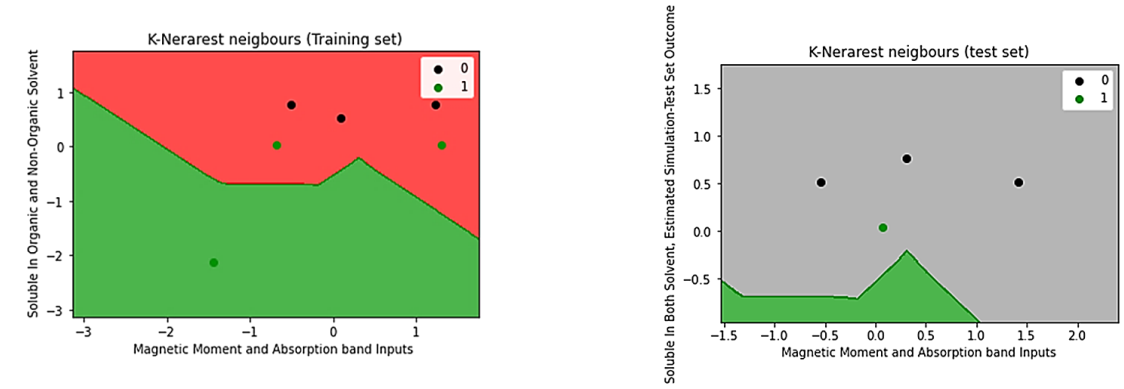

(a) K = 0

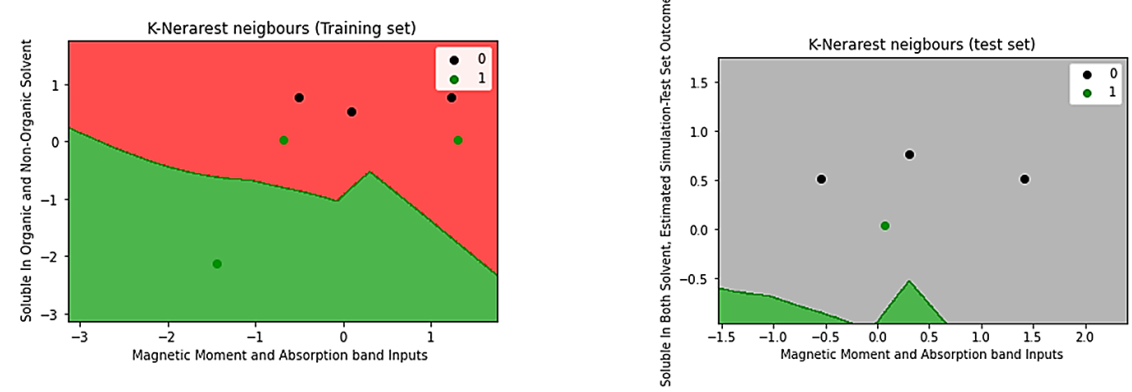

(b) K = 2

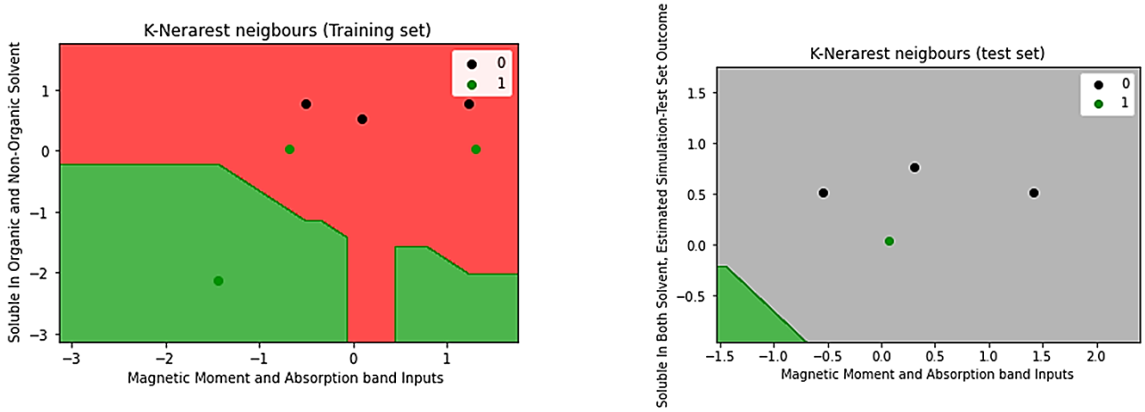

(c) K = 6

Figure 5. kNN training and testing data sets for (a) K = 0, (b) K = 2 , (c) K = 6 against 10 data sets points. Green indicates soluble complexes, and red indicates insoluble data points.

Parametric analysis of the characterization datasets of metal complexes showed interdependence. However, significantly characterization techniques are non-linear in relationship with the solubility among organic and inorganic solvents. The KNN machine learning algorithm accounts for the characterization datasets and solubility classification experimentation analysis. The data-driven ML model predicts a relationship between solubility and characterization techniques up to 75% precision. Biological fouling does not provide a significant data set, and no concrete relationship can be formulated statistically.

Disclosure statement

Conflict of interest: The authors declare that they have no conflict of interest.
Ethical approval: All ethical guidelines have been adhered to.
Sample availability: Samples of the compounds are available from the author.

CRediT authorship contribution statement

Conceptualization: Yousaf Arshad, Aqsa Rashid; Methodology: Yousaf Arshad, Aqsa Rashid; Software: Yousaf Arshad, Faisal Mahmood; Validation: Yousaf Arshad, Anam Suhail; Formal Analysis: Yousaf Arshad, Anam Suhail; Investigation: Yousaf Arshad, Aqsa Rashid; Resources: Yousaf Arshad, Salaha Saeed; Data Curation: Yousaf Arshad, Faisal Mahmood; Writing - Original Draft: Yousaf Arshad, Aqsa Rashid; Writing - Review and Editing: Yousaf Arshad, Anam Suhail; Visualization: Yousaf Arshad, Salaha Saeed; Supervision: Yousaf Arshad; Project Administration: Yousaf Arshad, Faisal Mahmood.

ORCID and Email

Muhammad Yousaf Arshad
yousaf.arshad96@yahoo.com
yousaf.arshad@interloop.com.pk
https://orcid.org/0000-0002-2081-0057

Aqsa Rashid
aqsaumer431@gmail.com
https://orcid.org/0000-0002-6913-917X
Faisal Mahmood
faisal.mahmood@uaf.edu.pk
https://orcid.org/0000-0003-4833-9225
Salaha Saeed
s.saeed.uet@gmail.com
https://orcid.org/0000-0002-4892-0581
Anam Suhail Ahmed
anamsuhail07@gmail.com
https://orcid.org/0000-0001-5481-2539

References

[1]. Mendil, D.; Uluözlü, O. D.; Tüzen, M.; Soylak, M. Investigation of the levels of some element in edible oil samples produced in Turkey by atomic absorption spectrometry. *J. Hazard. Mater.* **2009**, *165*, 724–728.
[2]. Aslantaş, M.; Kendi, E.; Demir, N.; Sabik, A. E.; Tümer, M.; Kertmen, M. Synthesis, spectroscopic, structural characterization, electrochemical and antimicrobial activity studies of the Schiff base ligand and its transition metal complexes. *Spectrochim. Acta A Mol. Biomol. Spectrosc.* **2009**, *74*, 617–624.
[3]. Al-Masoudi, N. A.; Aziz, N. M.; Mohammed, A. T. Synthesis andIn VitroAnti-HIV Activity of Some New Schiff Base Ligands Derived from 5-Amino-4-phenyl-4H-1,2,4-triazole-3-thiol and Their Metal Complexes. *Phosphorus Sulfur Silicon Relat. Elem.* **2009**, *184*, 2891–2901.
[4]. Deswal, Y.; Asija, S.; Kumar, D.; Jindal, D. K.; Chandan, G.; Panwar, V.; Saroya, S.; Kumar, N. Transition metal complexes of triazole-based bioactive ligands: synthesis, spectral characterization, antimicrobial, anticancer and molecular docking studies. *Res. Chem. Intermed.* **2022**, *48*, 703–729.
[5]. Aromí, G.; Barrios, L. A.; Roubeau, O.; Gamez, P. Triazoles and tetrazoles: Prime ligands to generate remarkable coordination materials. *Coord. Chem. Rev.* **2011**, *255*, 485–546.
[6]. Jin, X.; Xu, C.-X.; Yin, X.; He, P.; Zhang, J.-G. A 1D cadmium complex with 3,4-diamino-1,2,4-triazole as ligand: synthesis, molecular structure, characterization, and theoretical studies. *J. Coord. Chem.* **2015**, *68*, 1913–1925.
[7]. Haddad, R.; Yousif, E.; Ahmed, A. Synthesis and characterization of transition metal complexes of 4-Amino-5-pyridyl-4H-1,2,4-triazole-3-thiol. *Springerplus* **2013**, *2*, 510.
[8]. Haasnoot, J. G. Mononuclear, oligonuclear and polynuclear metal coordination compounds with 1,2,4-triazole derivatives as ligands. *Coord. Chem. Rev.* **2000**, *200–202*, 131–185.
[9]. Bräunlich, I.; Medvedev, M.; Dshemuchadse, J.; Wörle, M.; Caseri, W. Trinuclear Complexes of Nickel(II) and 4-Amino-1,2,4-triazole: Trinuclear Complexes of Nickel(II) and 4-Amino-1,2,4-triazole. *Z. Anorg. Allg. Chem.* **2015**, *641*, 2344–2349.
[10]. Fang, B.; Zhou, C.-H.; Rao, X.-C. Synthesis and biological activities of novel amine-derived bis-azoles as potential antibacterial and antifungal agents. *Eur. J. Med. Chem.* **2010**, *45*, 4388–4398.
[11]. Al-Soud, Y. A.; Al-Masoudi, N. A.; Ferwanah, A. E.-R. S. Synthesis and properties of new substituted 1,2,4-triazoles: potential antitumor agents. *Bioorg. Med. Chem.* **2003**, *11*, 1701–1708.
[12]. Bayrak, H.; Demirbas, A.; Karaoglu, S. A.; Demirbas, N. Synthesis of some new 1,2,4-triazoles, their Mannich and Schiff bases and evaluation of their antimicrobial activities. *Eur. J. Med. Chem.* **2009**, *44*, 1057–1066.
[13]. Kane, J. M.; Dudley, M. W.; Sorensen, S. M.; Miller, F. P. 2,4-Dihydro-3H-1,2,4-triazole-3-thiones as potential antidepressant agents. *J. Med. Chem.* **1988**, *31*, 1253–1258.
[14]. Karrouchi, K.; Chemlal, L.; Taoufik, J.; Cherrah, Y.; Radi, S.; El Abbes Faouzi, M.; Ansar, M. Synthesis, antioxidant and analgesic activities of Schiff bases of 4-amino-1,2,4-triazole derivatives containing a pyrazole moiety. *Ann. Pharm. Fr.* **2016**, *74*, 431–438.
[15]. Al-Shemary, R. K. Design, synthesis and biological evaluation of Schiff bases and their co(II), cu(II), Ni(II) chelates from derivative containing indole moiety bearing-triazole. *Eur. Chem. Bull.* **2017**, *6*, 433–439.
[16]. Gispert, J. R. *Coordination chemistry*; Wiley-VCH: Weinheim, Germany, 2008.
[17]. Zoubi, W. A. Biological activities of Schiff bases and their complexes: A review of recent works. *Int. J. Org. Chem. (Irvine)* **2013**, *03*, 73–95.
[18]. Turel, I. Special issue: Practical applications of metal complexes. *Molecules* **2015**, *20*, 7951–7956.
[19]. Zhang, G.-F.; Gao, L.; Li, P.; Zhao, F.-Q.; Fan, X.-Z.; Chen, N.; Xiang, X.-P.; Gao, H.-C.; Wang, J. Structural diversity in trinuclear nickel(II) complexes of 3,5-diamino-1,2,4-triazole. *J. Coord. Chem.* **2011**, *64*, 3551–3559.
[20]. Balouiri, M.; Sadiki, M.; Ibnsouda, S. K. Methods for in vitro evaluating antimicrobial activity: A review. *J. Pharm. Anal.* **2016**, *6*, 71–79.
[21]. Singh, K.; Kumar, Y.; Puri, P.; Sharma, C.; Aneja, K. R. Metal-based biologically active compounds: synthesis, spectral, and antimicrobial studies of cobalt, nickel, copper, and zinc complexes of triazole-derived schiff bases. *Bioinorg. Chem. Appl.* **2011**, *2011*, 901716.
[22]. Singh, K.; Kumar, Y.; Puri, P.; Sharma, C.; Aneja, K. R. Antimicrobial, spectral and thermal studies of divalent cobalt, nickel, copper and zinc complexes with triazole Schiff bases. *Arab. J. Chem.* **2017**, *10*, S978–S987.
[23]. Shakirova, O.G., Lavrenova, L.G., Shvedenkov, Y.G. Synthesis and Physicochemical Study of Iron(II), Cobalt(II), Nickel(II), and Copper(II) Complexes with 4-(2-Pyridyl)-1,2,4-Triazole. *Russian Journal of Coordination Chemistry* **2004**, *30*, 473–479.
[24]. Nfor, E. N.; Keenan, L. L.; Nenwa, J.; Ndifon, P. T.; Njong, R. N.; Dzesse, C. N. T.; Offiong, O. E. A novel mixed ligand dinuclear complex of cobalt (II): Synthesis, characterization and magnetic studies. *Cryst. Struct. Theory Appl.* **2014**, *03*, 22–29.
[25]. Raouf, H.; Beyramabadi, S. A.; Allameh, S.; Morsali, A. Synthesis, experimental and theoretical characterizations of a 1,2,4-triazole Schiff base and its nickel(II) complex. *J. Mol. Struct.* **2019**, *1179*, 779–786.
[26]. Tyagi, P.; Tyagi, M.; Agrawal, S.; Chandra, S.; Ojha, H.; Pathak, M. Synthesis, characterization of 1,2,4-triazole Schiff base derived 3d-metal complexes: Induces cytotoxicity in HepG2, MCF-7 cell line, BSA binding fluorescence and DFT study. *Spectrochim. Acta A Mol. Biomol. Spectrosc.* **2017**, *171*, 246–257.
[27]. Creaven, B. S.; Devereux, M.; Foltyn, A.; McClean, S.; Rosair, G.; Thangella, V. R.; Walsh, M. Quinolin-2(1H)-one-triazole derived Schiff bases and their Cu(II) and Zn(II) complexes: Possible new therapeutic agents. *Polyhedron* **2010**, *29*, 813–822.
[28]. Ugryumov, I. A.; Ilyushin, M. A.; Tselinskii, I. V.; Kozlov, A. S. Synthesis and Properties of Photosensitive Complex Perchlorates of d Metals with 3(5)-Hydrazino-4-amino-1,2,4-triazole as Ligand. *Russ. J. Appl. Chem.* **2003**, *76*, 439–441.
[29]. Bharty, M. K.; Bharati, P.; Bharti, A.; Singh, A.; Singh, S.; Singh, N. K. Syntheses, spectral and structural characterization of Ni(II) complexes of 4-amino-5-phenyl/3-pyridyl/thiophen-2H-1,2,4-triazole-3-thione. *J. Mol. Struct.* **2014**, *1056–1057*, 326–332.
[30]. Xin, Y. I. N.; Xin, J. I. N.; Cai-Xia, X. U.; Piao, H. E.; Wang, K.; Zhang, J.-G. Synthesis and characterization of four energetic transition metal complexes of 3, 4-diamino-1, 2, 4-triazole. *Central European Journal of Energetic Materials 13*, 301–320.
[31]. Zhang, Y.-L.; Chen, S.-P.; Gao, S.-L. Synthesis and characterization of new M-triazole complexes (M = co, cu, Zn). *Z. Anorg. Allg. Chem.* **2009**, *635*, 537–543.
[32]. Nabipour, H.; Wang, X.; Song, L.; Hu, Y. Facile synthesis of a novel zinc-triazole complex for simultaneous improvement in fire safety and mechanical properties of epoxy resins. *Compos. Part A Appl. Sci. Manuf.* **2021**, *143*, 106284.
[33]. Singh, K.; Singh, D. P.; Barwa, M. S.; Tyagi, P.; Mirza, Y. Antibacterial Co(II), Ni(II), Cu(II) and Zn(II) complexes of Schiff bases derived from fluorobenzaldehyde and triazoles. *J. Enzyme Inhib. Med. Chem.* **2006**, *21*, 557–562.
[34]. Gaber, M.; El-Wakiel, N. A.; El-Ghamry, H.; Fathalla, S. K. Synthesis, spectroscopic characterization, DNA interaction and biological activities of Mn(II), Co(II), Ni(II) and Cu(II) complexes with [(1H-1,2,4-triazole-3-ylimino)methyl]naphthalene-2-ol. *J. Mol. Struct.* **2014**, *1076*, 251–261.
[35]. Zhang, X.-Y.; Liu, Z.-Y.; Xia, Y.-F.; Zhang, Y.-Y.; Yang, E.-C.; Zhao, X.-J. Three 3-amino-1,2,4-triazole-based cobalt(II) complexes incorporating with different carboxylate coligands: synthesis, crystal structures, and magnetic behavior. *J. Coord. Chem.* **2013**, *66*, 4399–4414.
[36]. Singh, A. K.; Pandey, O. P.; Sengupta, S. K. Synthesis, spectral characterization and biological activity of zinc(II) complexes with 3-substituted phenyl-4-amino-5-hydrazino-1, 2, 4-triazole Schiff bases. *Spectrochim. Acta A Mol. Biomol. Spectrosc.* **2012**, *85*, 1–6.
[37]. Nagendra Prasad, H. S.; Karthik, C. S.; Mallesha, L.; Mallu, P. A short review on biological activity of triazole containing metal complexes. *Asian Journal of Pharmaceutical Analysis and Medicinal Chemistry* **2014**, *2*, 214–229.
[38]. Altalbawy, F. M. A.; Mohamed, G. G.; Abou El-Ela Sayed, M.; Mohamed, M. I. A. Synthesis, characterization, and biological activity of some transition metal complexes with Schiff base ligands derived from 4-amino-5-phenyl-4H-1,2,4-triazole-3-thiol and salicaldehyde. *Monatsh. Chem.* **2012**, *143*, 79–89.
[39]. Arshad, Y. M.; Rashid, A.; Gul, H.; Ahmad, A. S.; Jabbar, F. Optimization of acid-assisted extraction of pectin from banana (Musa Acuminata) peels by central composite design. *Glob. NEST J.* **2022**, *24*, 752–756.
[40]. Dhomse, B. K.; Mahale, M. K. Study of machine learning algorithms for special disease prediction using principal of component analysis. In *2016 International Conference on Global Trends in Signal Processing, Information Computing and Communication (ICGTSPICC)*; IEEE, 2016.

[41]. Musumeci, F.; Rottondi, C.; Nag, A.; Macaluso, I.; Zibar, D.; Ruffini, M.; Tornatore, M. An overview on application of machine learning techniques in optical networks. *IEEE Commun. Surv. Tutor.* **2019**, *21*, 1383–1408.
[42]. Berk, R. A.; Sorenson, S. B.; Barnes, G. Forecasting domestic violence: A machine learning approach to help inform arraignment decisions: Forecasting domestic violence. *J. Empir. Leg. Stud.* **2016**, *13*, 94–115.
[43]. Saeed, M. A.; Niedzwiecki, L.; Arshad, M. Y.; Skrinsky, J.; Andrews, G. E.; Phylaktou, H. N. Combustion and explosion characteristics of pulverised wood, valorized with mild pyrolysis in pilot scale installation, using the modified ISO 1 m3 dust explosion vessel. *Appl. Sci. (Basel)* **2022**, *12*, 12928.
[44]. Zhang, S.; Cheng, D.; Deng, Z.; Zong, M.; Deng, X. A novel k NN algorithm with data-driven k parameter computation. *Pattern Recognit. Lett.* **2018**, *109*, 44–54.
[45]. Gul, H.; Arshad, M. Y.; Tahir, M. W. Production of H2 via sorption enhanced auto-thermal reforming for small scale Applications-A process modeling and machine learning study. *Int. J. Hydrogen Energy* **2023**, https://doi.org/10.1016/j.ijhydene.2022.12.217.
[46]. Sharma, S.; Sharma, D. Intelligently applying artificial intelligence in chemoinformatics. *Curr. Top. Med. Chem.* **2018**, *18*, 1804–1826.
[47]. Cordeiro de Amorim, R.; Makarenkov, V.; Mirkin, B. A-Ward pβ : Effective hierarchical clustering using the Minkowski metric and a fast k -means initialisation. *Inf. Sci. (Ny)* **2016**, *370–371*, 343–354.
[48]. Piotrowski, Z.; Szypulska, M. Classification of falling asleep states using HRV analysis. *Biocybern. Biomed. Eng.* **2017**, *37*, 290–301.
[49]. Yar, A.; Arshad, M. Y.; Asghar, F.; Amjad, W.; Asghar, F.; Hussain, M. I.; Lee, G. H.; Mahmood, F. Machine learning-based relative performance analysis of monocrystalline and polycrystalline grid-tied PV systems. *Int. J. Photoenergy* **2022**, *2022*, 1–18, 3186378